Conformation of the c-Fos/c-Jun Complex In Vivo: A Combined FRET, FCCS, and MD-Modeling Study

György Vámosi,* Nina Baudendistel,† Claus-Wilhelm von der Lieth,‡ Nikoletta Szalóki,* Gábor Mocsár,* Gabriele Müller,† Péter Brázda,§ Waldemar Waldeck,† Sándor Damjanovich,* Jörg Langowski,† and Katalin Tóth†

*Cell Biology and Signaling Research Group of the Hungarian Academy of Sciences, Department of Biophysics and Cell Biology, Medical and Health Science Center, University of Debrecen, Debrecen, Hungary; †Biophysics of Macromolecules Division, ‡Spectroscopic Department, Molecular Modeling, German Cancer Research Center, Heidelberg, Germany; and §Department of Biochemistry and Molecular Biology, Medical and Health Science Center, University of Debrecen, Debrecen, Hungary

ABSTRACT The activator protein-1 transcription factor is a heterodimer containing one of each of the Fos and Jun subfamilies of basic-region leucine-zipper proteins. We have previously shown by fluorescence cross-correlation spectroscopy (FCCS) that the fluorescent fusion proteins Fos-EGFP and Jun-mRFP1, cotransfected in HeLa cells, formed stable complexes in situ. Here we studied the relative position of the C-terminal domains via fluorescence resonance energy transfer (FRET) measured by flow cytometry and confocal microscopy. To get a more detailed insight into the conformation of the C-terminal domains of the complex we constructed C-terminal labeled full-length and truncated forms of Fos. We developed a novel iterative evaluation method to determine accurate FRET efficiencies regardless of relative protein expression levels, using a spectral- or intensity-based approach. The full-length C-terminal-labeled Jun and Fos proteins displayed a FRET-measured average distance of 8 ± 1 nm. Deletion of the last 164 amino acids at the C-terminus of Fos resulted in a distance of 6.1 ± 1 nm between the labels. FCCS shows that Jun-mRFP1 and the truncated Fos-EGFP also interact stably in the nucleus, although they bind to nuclear components with lower affinity. Thus, the C-terminal end of Fos may play a role in the stabilization of the interaction between activator protein-1 and DNA. Molecular dynamics simulations predict a dye-to-dye distance of 6.7 ± 0.1 nm for the dimer between Jun-mRFP1 and the truncated Fos-EGFP, in good agreement with our FRET data. A wide variety of models could be developed for the full-length dimer, with possible dye-to-dye distances varying largely between 6 and 20 nm. However, from our FRET results we can conclude that more than half of the occurring dye-to-dye distances are between 6 and 10 nm.

INTRODUCTION

The transcription factors c-Fos and c-Jun participate in the regulation of several cellular processes including proliferation, differentiation, apoptosis, and oncogenesis (1–3). They fulfill their function as dimers; we note, however, that although Jun can act both as a homodimer and a heterodimer with Fos, Fos does not form homodimers. The complex binds to activator protein-1 (AP-1) binding sites in the promoter or enhancer regions of several mammalian genes. The known x-ray crystallographic structure of the Jun-Fos dimer is limited to only the basic DNA binding and the adjacent dimerization (bZip or leucine zipper) domains of each protein (4) (see Fig. 1 *A*). No crystallographic data are available about either the N-terminal transactivation domains or the C-terminal segments.

Jun and Fos interact as a heterodimer in vitro and in vivo. Our previous work using fluorescence cross-correlation spectroscopy (FCCS) demonstrated that the two hybrid proteins, Fos-EGFP and Jun-mRFP1, interact in vivo in the nucleus. The cross-correlation curve was dominated by a slow component, indicating that the majority of the interactions took place while the proteins were bound to DNA. While FCCS is a very powerful technique for demonstrating the interaction between two binding partners in vivo or in vitro (5–7), it does not yield any quantitative information on the distance of the two interacting partners. Fluorescence resonance energy transfer (FRET), on the other hand, can be used for quantitative distance determinations between two fluorophores in the range of 2–10 nm both in vitro and in vivo (8–12). When performing accurate distance measurements using FRET, careful analysis procedures must be applied, which account for background fluorescence, spectral cross-talk between detection channels, relative excitation and detection efficiency of donor and acceptor signals, and quantum yields of the fluorophores (13).

Labeling Jun and Fos with autofluorescent proteins facilitates in vivo distance measurements between the different domains, complementing the limited information from crystallography. Experiments using photobleaching FRET (pbFRET) and FLIM FRET (14) showed a measurable FRET efficiency (7.5%), implying a <10 nm distance between the N-termini (transactivation domains), although there is a difference of $\sim$120 amino acids (AAs) between them with respect to the DNA binding site. Also, bimolecular fluorescence complementation (BiFC) experiments demonstrated that not only sites quasi-juxtaposed (10–17 AAs) from the C-terminal end of the dimerization domain are close enough for BiFC, but

Submitted September 9, 2007, and accepted for publication November 20, 2007.

Address reprint requests to Katalin Tóth, Tel.: 49-6221-42-3390; E-mail: kt@dkfz.de.

Editor: David P. Millar.

0006-3495/08/04/2859/10 $2.00

doi: 10.1529/biophysj.107.120766

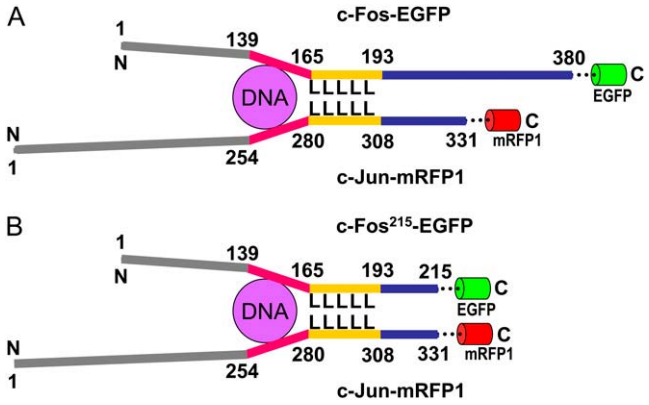

FIGURE 1 Schematic drawing of the Fos-Jun dimers. Domain structure (from *left* to *right*): N-terminal transactivation domain; DNA-binding domain; dimerization domain with leucine zipper (LLLLL); C-terminal domain; 5–7 AA linker; and fluorescent tag. (*A*) The C-terminal domain of the full-length Fos-EGFP is 164-AAs longer than that of Jun-mRFP1. (*B*) The truncated C-terminal domain of c-Fos^{215}-mRFP1 is in register with that of Jun-mRFP1. The scheme does not represent the true geometry, it is just meant to visualize the domain structure of the proteins (based on (19)).

also the, linearly, very distant N-terminus of Fos and the C-terminus of Jun can form such a complex (15). BiFC is an indisputably simple and reliable indicator of protein-protein interactions; however, by binding the labeled moieties together, the native conformation and thermodynamic equilibrium parameters of the complex can be skewed; therefore, it cannot be used for distance measurements (16,17).

Previously, we labeled Fos and Jun proteins at their C-terminal ends (18). To characterize the relative distances of the various domains within the complex, we determined the FRET efficiency between them by flow cytometry and confocal microscopy. Since the Fos C-terminal domain is 164 AAs in length longer than that of Jun, when counted from the end of the dimerization domain (19), we also constructed a truncated Fos moiety (Fos^{215}-EGFP) to gain distance information between another pair of points of the C-terminal domains. To check whether the truncation affects the mobility, dimerization, or DNA binding, we measured FCCS with our modified molecules, and compared them to the results obtained with the full-length molecules.

We used two intensity-based FRET approaches: a cell-by-cell measurement using flow cytometry (FACS) and pixel-by-pixel measurement using confocal microscopy. Both methods are calculation-intensive, but have special advantages when compared to the relatively simple and robust pbFRET. For example, when using flow cytometric FRET, tens of thousands of cells can be measured in a few minutes providing superior statistics. In our confocal microscopic method, the different fluorescence signals from any given pixel are collected almost simultaneously. The time lapse between different channels is only a few milliseconds, which minimizes artifacts that arise from diffusion of the labeled molecules or movement of the cell, where pbFRET uses longer measurement time (several tens of seconds) resulting in blurring of the FRET image. We have developed a novel iterative method for the determination of accurate FRET efficiencies in whole cells based on the measurement of donor, transfer, and acceptor signals. With this method, we can determine not only the pixel-by-pixel or cell-by-cell value of the FRET efficiencies, but also the relative acceptor-to-donor expression levels. For calibrating the acceptor/donor ratio, we used a single sample expressing a fusion protein consisting of a donor and an acceptor moiety.

Using molecular dynamics simulations based on known crystal structures and subsequent energy minimization of the Fos-Jun dimer and the autofluorescent proteins, we determined plausible conformations for the C-terminal domains. The compatibility of the proposed structures with the FRET-measured distances is discussed.

MATERIALS AND METHODS

Plasmid constructions

Expression constructs for fusion proteins were designed into the parent pSV-EYFP vector originating from pECFP-1 (BD Biosciences, Palo Alto, CA). To drive overexpression of the protein constructs, the SV40 promoter sequence was inserted into the *Hin*d III restriction site. Expression vectors pSV-c-Jun-mRFP1 and pSV-c-Fos-EGFP were constructed using a multistep cloning strategy as previously described in Baudendistel et al. (18) and cloned into the expression vector described above. Briefly, pSV-c-Jun-mRFP1 consists of full-length human Jun fused to mRFP1 with the linker sequence RDPPV cloned to create the protein Jun-mRFP1. pSV-c-Fos-EGFP consists of full-length human Fos fused to EGFP with a linker sequence RDPPVAT. The resulting fusion proteins are referred to as Fos-EGFP and Jun-mRFP1 in the text.

Fos^{215}-EGFP is a truncated version of Fos-EGFP whereby the last 164 amino acids have been removed. The vector pSV-c-Fos^{215}-EGFP contains the expression construct for this protein and was generated by amplifying the coding sequence of the human c-Fos gene by polymerase chain reaction with the following primers: 5′-CTT CGA ATT CTG ATG ATG TTC TCG GGC TTC AAC GC-3′ and 5′-AAT TTA TGG ATC CCG CTC TTC TGG GAA GCC CAG GTC-3′. The amplified fragment was inserted into the plasmid as described for full-length Fos-EGFP (18). The resulting protein termed Fos^{215}-EGFP contains 215 amino acids of the original sequence. A schematic drawing of the domain structure of the Jun-Fos heterodimers is presented in Fig. 1.

We constructed a deletion mutant of c-Jun lacking the DNA-binding and dimerization domains (18), which codes for the first 145 amino acids of c-Jun and the sequence of mRFP1 at the C-terminal (JunΔ-mRFP1). Coexpression of this mutant with Fos-EGFP or Fos^{215}-EGFP served as a negative control for dimerization studies.

The control vectors pSV-EGFP-mRFP1 (coding for a fusion protein of the two dyes separated by a 7-AA linker), and the bicistronic pIRES2-EGFP-mRFP1 (expressing the dyes separately) were generated as previously described (18). The products expressed from these vectors served as positive and negative controls for our FRET measurements.

Cell culture

Adherent HeLa cells (provided by F. Rösl, DKFZ, Heidelberg, Germany) were grown in a 5% CO_2 humidified atmosphere in RPMI 1640 without phenol red (Invitrogen Life Technologies, Carlsbad, CA) and supplemented with 10% (v/v) fetal calf serum. Transfections with the mammalian ex-

pression vectors were carried out with Transfectin (BioRad Laboratories, München, Germany) as proposed by the manufacturers (2 μg DNA for 4.5 μl Transfectin). Cotransfections with the vectors pSV-c-Fos-EGFP and pSV-c-Jun-mRFP1 were transfected together in an optimized 1:4 ratio. For FRET and fluorescence correlation spectroscopy (FCS) imaging, HeLa cells were plated and transfected in eight-well chambered LabTek coverslips (Nunc, Wiesbaden, Germany) and measured at room temperature. For flow cytometric FRET experiments, cells were cultured subconfluent, transfected in the flasks, trypsinized, washed twice, and resuspended in Hanks solution.

Determination of FRET by flow cytometry

Flow cytometric FRET measurements were carried out on a FACSDIVA instrument (Becton Dickinson, San Jose, CA). Forward and side scattering were used to sort out debris and apoptotic cells. FRET efficiency between EGFP and mRFP1 was determined on a cell-by-cell basis by applying the procedure described previously (13) with the following modifications. For the excitation of EGFP and mRFP1, the 488-nm line of an Innova 90 Ar ion laser (Coherent, Los Gatos, CA) and the 532-nm line of a stabilized solid-state laser were used. Due to the spatial separation between the laser foci, fluorescence signals excited by the two lasers could be detected separately. Three signals were measured in independent channels from each cell: I_1 (donor signal), I_2 (FRET signal), and I_3 (acceptor signal). These fluorescence intensities can be expressed by the following set of equations in terms of contributions due to direct excitation of the donor and the acceptor, sensitized emission of the acceptor, and cellular autofluorescence:

$$\begin{aligned} I_1(488, 500-540) &= I_D(1-E) + B_1 \\ I_2(488, 597-639) &= I_D(1-E)S_1 + I_A S_2 + I_D E\alpha + B_2 \\ I_3(532, 597-639) &= I_A + B_3. \end{aligned} \quad (1)$$

The brackets refer to the wavelengths of excitation and detection. I_D is the unquenched donor signal in channel 1 that would be measured in the absence of acceptor, I_A is the acceptor signal in channel 3, and E is the mean FRET efficiency in the given cell. B_1, B_2, and B_3 are the average nonspecific autofluorescence contributions in the respective channels, which were determined as the mean intensities from nontransfected HeLa cells. The spectral crosstalk factor S_1 was calculated using cells expressing EGFP as

$$S_1 = (I_2 - B_2)/(I_1 - B_1). \quad (2)$$

S_2 was measured from cells expressing mRFP1 only:

$$S_2 = (I_2 - B_2)/(I_3 - B_3). \quad (3)$$

The factor α, which relates the signal arising from the fluorescence of any given number of excited EGFP molecules in channel 1 to that from an equal number of excited mRFP1 molecules in channel 2, is defined by the equation

$$\alpha = \frac{Q_A \eta_A}{Q_D \eta_D}, \quad (4)$$

where Q_D and Q_A are the fluorescence quantum yields of EGFP and mRFP1, and η_A and η_B are the detection efficiencies (including emission filter transmissions, detector sensitivities, and amplifications) of the donor and acceptor fluorescence emission in channels 1 and 2, respectively. Technically, the value of α can be determined from two samples expressing known amounts of EGFP or mRFP1 by using the expression

$$\alpha = \frac{I_2^A}{I_1^D} \frac{\varepsilon^D(488)}{\varepsilon^A(488)} \frac{N^D}{N^A}, \quad (5)$$

where I_2^A is the directly excited fluorescence of the acceptor, I_1^D is the fluorescence emission of the donor, $\varepsilon^D(488)$ ~53,000 M^{-1} cm^{-1} (20) and $\varepsilon^A(488)$ ~4030 M^{-1} cm^{-1} (L. C. Robinson, University of Minnesota, Minneapolis, personal communication, 2007) are the extinction coefficients of the donor and the acceptor at 488 nm, and N^D/N^A is the ratio of donor and acceptor fluorophores expressed by the samples. Knowing S_1, S_2, and α, Eq. 1 can be solved for E, I_D, and I_A for each cell:

$$E = 1 - \frac{1}{1 + \frac{1}{\alpha}\left(\frac{(I_2 - B_2) - S_2(I_3 - B_3)}{I_1 - B_1} - S_1\right)}. \quad (6)$$

However, the calculation of α for EGFP- and mRFP1-labeled proteins poses a problem because it is not straightforward to determine the ratio of the expression levels of EGFP and mRFP1 in distinct cell populations. Even if using a bicistronic plasmid (e.g., IRES), from which the genes of both fluorophores are transcribed in the same cell, the ratio of the expression level of EGFP to that of mRFP1 is different than 1 (~0.2) because the two proteins are transcribed from distinct promoters and are processed independently. Therefore, we assessed α by using cells expressing the EGFP-mRFP1 fusion protein, in which the ratio N^D/N^A is 1. Since FRET occurs between the donor and acceptor moieties of the fusion proteins, the unquenched I_D donor intensity, and the directly excited acceptor fluorescence I_A cannot be determined directly from this sample. Therefore, a successive approximation method was used for the determination of α and E simultaneously. Since $I_2^A = (I_3 - B_3) \times S_2$, and $I_D = (I_1 - B_1)/(1 - E)$, for α we can write

$$\alpha = \frac{(I_3 - B_3) \times S_2 \times (1 - E)}{I_1 - B_1} \times \frac{\varepsilon^D(488)}{\varepsilon^A(488)}. \quad (7)$$

In the first approximation of α, $E = 0$ was assumed, and the resulting α-value was used for calculating E for the fusion protein by Eq. 6. The resulting mean E value was then substituted into Eq. 7, and the next approximation for α was derived. This way convergence to the optimized E- and α-values was achieved in five iterations. Average cell-by-cell FRET efficiencies were plotted as frequency distribution histograms. Data were evaluated using the softwares AFLEX and REFLEX developed for flow cytometric FRET measurements at our department (21).

The acceptor/donor expression ratio was determined in the cotransfected samples by the following procedure. Using the EGFP-mRFP1 sample, the FRET-corrected fluorescence ratio of the acceptor and the donor was calculated:

$$Q = \frac{(I_3 - B_3) \times (1 - E)}{(I_1 - B_1)}. \quad (8)$$

For other cotransfected cells, the acceptor-to-donor expression ratio N^A/N^D was assessed as

$$N_A/N_D = \frac{(I_3 - B_3) \times (1 - E)}{(I_1 - B_1) \times Q}. \quad (9)$$

Confocal microscopy

FRET measurements on a pixel-by-pixel basis were performed on an LSM 510 confocal microscope (Carl Zeiss, Jena, Germany). Excitation was performed by using the 488-nm line of an Ar ion and the 543-nm line of a HeNe laser. The 1.5-μm-thick optical slices across the nucleus were then scanned, and three signals: donor (excitation: 488 nm, emission: 500–550 nm), FRET (excitation: 488 nm, emission: 560–610), and acceptor channel (excitation: 543 nm; emission: 560–610 nm) were collected. The ''Multi Track'' option of the data acquisition software using alternating laser illumination was used to minimize spectral overspill between the channels. Images were low-pass filtered and corrected for pixel shift between the channels, if necessary, using the LSM data acquisition software. Further processing and evaluation of FRET efficiencies on a pixel-by-pixel basis was performed using the SCILIMAGE software. Average background intensities were determined

from nontransfected cells. Images were background-corrected, and pixels above the threshold (~2× background) were further analyzed. FRET efficiencies were calculated analogous to the procedure described for flow cytometry. Results were displayed as false-color images of pixel-by-pixel FRET efficiency maps, as well as in the form of pixel frequency distribution histograms. Average FRET efficiencies were calculated from 80 cells.

Fluorescence correlation spectroscopy (FCS)

We recorded confocal images and carried out auto- and cross-correlation measurements at selected points of cells (with a positioning accuracy of 30 nm) on a homebuilt setup that combines an FCS module and a beam scanning unit attached to the video port of an inverted microscope (IX-70, Olympus, Melville, NY) (22–24). EGFP fluorescence was excited with the 488 nm line of an Ar-Kr laser (Omnichrome, Melles Griot, Bensheim, Germany) and detected from 515 nm to 545 nm, whereas the mRFP1 fluorescence was excited with the 568 nm line of the same laser and detected between 608 nm and 635 nm. Fluorescence was detected by avalanche photodiodes (SPCM-AQR-13, Perkin-Elmer, Wellesley, MA) used in photon counting mode. For FCS and FCCS the detector signal is fed into an ALV-5000/E correlator card (ALV Laser, Langen, Germany), which records the time course of the signal and calculates its autocorrelation function in real time. FCS and FCCS measurements were performed at 23°C at laser intensities between 5 and 10 kW/cm^2. Data acquisition time at a selected point was 60 s, consisting of 6 × 10 s runs; the correlation functions were then averaged. Auto- and cross-correlation curves were fit to a model assuming two freely diffusing components, and a triplet term for the autocorrelation curves (18). The confocal volume was characterized by measuring fluorescein and ALEXA 568 dyes (Invitrogen), dissolved in 10 mM Tris, 0.1 mM EDTA, 5 mM NaCl, pH 7.5 buffer.

Construction of an atomic model of the Fos-Jun adduct

The goal of the modeling study was to generate a realistic three-dimensional model of the Jun-Fos molecular structure, therefore giving us insight into the proximity limits between the two chromophores. The model of the Fos/Fos^{215}-EGFP + Jun-mRFP1 dimers downstream of the DNA binding domains (from residues 139 for Fos and 254 for Jun), plus the short linkers and the fluorophores was constructed on the basis of experimentally determined three-dimensional folds taken from the Protein Database (PDB) (4,25,26). Missing connections between domains were approximated by selecting either reasonable templates from the PDB or by setting a manually constructed short sequence to a preferable secondary structural motif. The constructed molecules were subsequently relaxed using force-field methods.

The base of our modeling studies used a crystal structure of the Jun/Cre complex (residues 254–315, Cre/cAMP response element on the DNA, PDB-entry 1JNM, resolution 2.2 Å). The DNA and all water molecules were then removed, and the nonidentical amino acids were manually exchanged corresponding to the target sequence. For the remaining sequence of Jun-mRFP1 (residues 316–330: VNGSCQLMTQQLQTF), we performed a FASTA search in the PDB to find similar motifs. In our models we substituted a motif from the putative glycine cleavage system Transcriptional Repressor structure (PDB-Entry 1U8S: 58% identity in 12-AA overlap); the nonidentical amino acids were manually replaced according to the target sequence.

The same procedure was applied to the Fos^{215}-EGFP strand (residues 139–198) and for the remaining AHRPACKIPDDLGFPEE (199–215), for which a motif from the Human Tff1 3D Structure (PDB-entry 1HI7 with 47% identity in 15-AA overlap) was extracted. Modeling of the Fos protein with full-length C-terminal needed more extensive protein structure prediction and additional molecular modeling approaches. As a first step, the C-terminal domain of Fos was sent to the PredictProtein (Rost) service for sequence analysis and structure prediction (cubic.bioc.columbia.edu/predictprotein/). Other protein structure prediction and homology modeling services were also used. Full atomic models were generated by using SWISS-MODEL (27); nonconnected parts of the generated structures were manually attached using the INSIGHT II software to handle three-dimensional molecular structures. Subsequently, the structures were optimized with the CVFF force field using the DISCOVER program. The so-derived potential structures of the C-terminal domain of Fos were then successively manually inserted into the existing Fos^{215}-EGFP/Jun-mRFP construct before the EGFP.

The short linkers between Jun and Fos and the subsequent fluorescent proteins were manually constructed, as was the pentapeptide with the sequence MASSE (336–340), which was missing in the crystal structure of mRFP1. The nonidentical amino acids were replaced in mRFP (based on PDB entry 1G7K (25) as template: 83% sequence identity in 219 AAs) and EGFP (based on PDB 1GFL (26) as template: 98% identity in 237 AAs) using the optimize mode of the SWISS-Model protein structure homology-modeling server. All generated templates were relaxed with a short force-field optimization and subsequently manually connected. All manipulations of the three-dimensional structures were accomplished with the INSIGHTII interface. The constructed complex was then optimized assigning the potentials of the CVFF force field as required for DISCOVER.

The construct Fos^{215}-EGFP + Jun-mRFP1 was optimized using the all-atom force field GROMACS software package (28) in a water box with explicit water molecules in a volume of 189 × 125 × 131 Å. The total number of atoms was ~3×10^5 (~10^5 water molecules); the Fos^{215} + Jun adducts consisted of 6.3×10^3 atoms. The integration time step was 10^{-15} s at a simulation temperature of 300 K. Particle-mesh Ewald summation was used to account for the electrical attractions and repulsions between nonbonded atoms. A total of 550 ps were simulated. No additional constraints were applied.

RESULTS AND DISCUSSION

FRET

To investigate the relative positions of the labeled molecular moieties of the transcriptional activator AP-1 in vivo, we performed FRET experiments by two separate methods, flow cytometry and confocal microscopy.

We used the fluorescent fusion proteins Fos-EGFP and Jun-mRFP1 shown in Fig. 1 *A*. In these constructs, full-length Jun and Fos were fused with fluorescent proteins mRFP1 and EGFP, respectively, to their C-termini. The structure of the domains downstream of the leucine zipper is unknown. The C-terminal moiety of Fos is 165-amino-acids longer than that of Jun. To get distance information also from the internal parts of the Fos C-terminal domain, we moved the EGFP closer to the dimerization domain by truncating the Fos-EGFP construct (termed Fos^{215}-EGFP Fig. 1 *B*), resulting in equally long C-termini.

As a negative control for dimerization, we used samples cotransfected with Fos-EGFP/Fos^{215}-EGFP and JunΔ-mRFP1, a mutant lacking the DNA-binding and dimerization domains at the C-terminal. As another negative control, cells expressing EGFP and mRFP1 separately from the bicistronic IRES vector were used. As a positive control for FRET, the fusion protein of EGFP and mRFP1 was applied. In this construct, the two fluorophores are only separated by a 7-AA-long spacer, and are expressed in a 1:1 ratio.

Fig. 2 shows the dependence of the FRET efficiency on the acceptor/donor ratio (N_A/N_D) measured on a cell-by-cell basis by FACS. For the EGFP-mRFP1 fusion protein, the

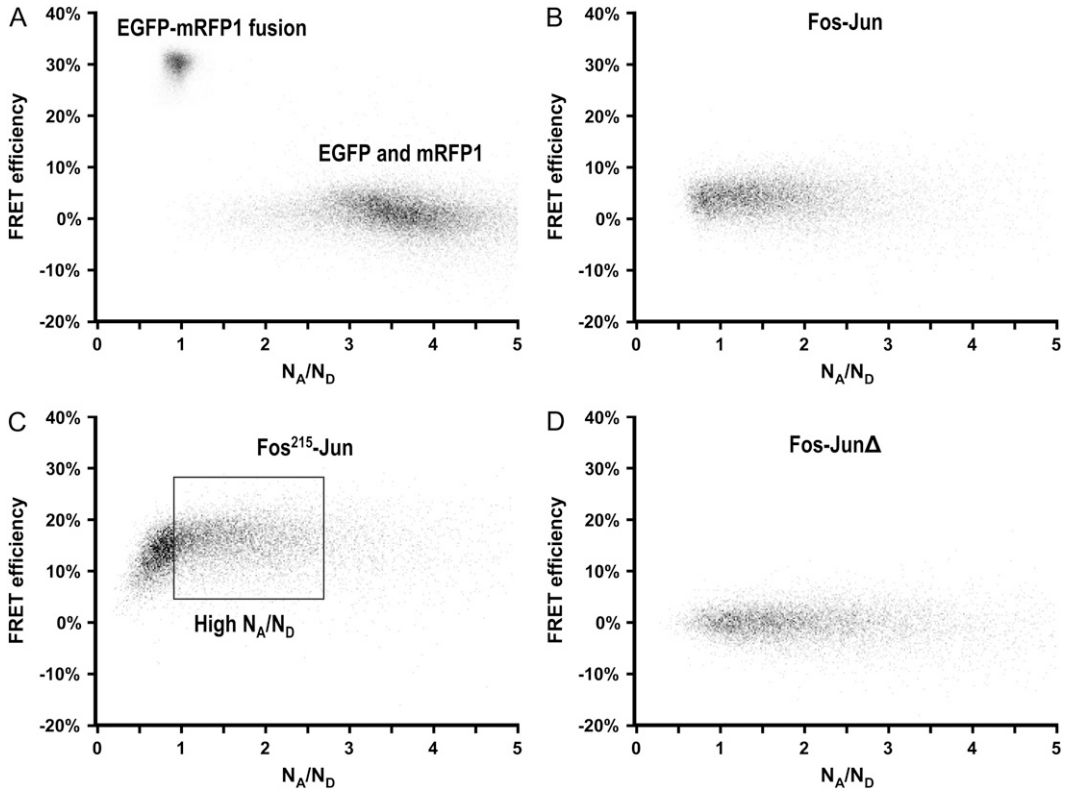

FIGURE 2 Mean cellular FRET efficiencies versus acceptor/donor ratios measured by flow cytometry as determined from >20,000 cells. (*A*) Positive and negative controls: EGFP-mRFP1 fusion protein and EGFP and mRFP1 expressed separately. (*B*) Full-length Fos-EGFP + Jun-mRFP1. (*C*) Truncated Fos^{215}-EGFP+Jun-mRFP1. (*D*) Fos-EGFP and JunΔ-mRFP1 (dimerization/DNA-binding deletion mutant).

value of N_A/N_D should be 1 by definition. The FRET efficiency is centered at ~30%. The obtained distribution is symmetric and narrow along both axes (Fig. 1 *A*); the widths illustrate the errors due to the uncertainty of the parameters involved in their derivation. For the separately expressed EGFP and mRFP1 sample, the expression efficiencies of the two dyes are significantly different (N_A/N_D is centered at ~4), and the average FRET efficiency is distributed around zero as expected. For the Fos-Jun dimers, the distributions of N_A/N_D are wide due to the cell-to-cell variability of the expression efficiency from the cotransfected vectors. The FRET efficiency values do not vary according to the value of N_A/N_D for the full-length dimer; the average is ~4% (Fig. 2 *B*). For the Fos^{215}-Jun dimer, the FRET efficiency is constant (~17%) for N_A/N_D values >1 (gated high N_A/N_D region in Fig. 2 *C*), and decreases with decreasing N_A/N_D due to the presence of more donor-labeled Fos^{215} molecules having no acceptor-labeled Jun partner. The FRET efficiency of the nonassociating deletion mutant Fos + JunΔ sample, a biologically relevant negative control, displays a narrow distribution around zero (Fig. 2 *D*).

Histograms shown in Fig. 3 demonstrate the cell-by-cell distributions of the FRET efficiency for all samples. For the Fos^{215}-Jun sample, only cells in the high N_A/N_D region were included, corresponding to cells with the overwhelming majority of Fos^{215} in complex with Jun. The mean values of the FRET efficiencies are 0.5 ± 1% for the Fos-JunΔ, 4 ± 0.5% for the full-length Fos-Jun, and 17 ± 1% for the Fos^{215}-Jun samples (Fig. 3 *A*). The following mean values were obtained for the controls: 0% for the cells expressing EGFP alone, 0.2 ± 2% for the separately expressed EGFP + mRFP1 samples, and 30 ± 1% for the EGFP-mRFP1 fusion (Fig. 3 *B*). The measured energy transfer efficiencies, which may be averages over ensembles of possible conformations, correspond to average dye-to-dye distances of 8 ± 1 nm for the full-length Fos-Jun, 6.1 ± 1 nm for the truncated Fos^{215}-Jun, and 5.4 ± 0.5 nm for the EGFP-mRFP1 fusion sample. In these calculations we assumed a κ^2 of 2/3 and a Förster radius of 4.7 ± 0.5 nm (29,30).

Flow cytometric energy transfer experiments have excellent statistics due to the high number of measured cells, but they do not provide information at the subcellular level. We used confocal microscopic FRET analysis to resolve any possible spatial inhomogeneities of probe concentration and protein-protein interactions. The spatial resolution of the technique is ~200 nm. Fig. 4 shows representative confocal images of cells. Fos^{215} and Jun (*top row*) as well as full-length Fos (data not shown) were distributed evenly in the whole nucleus contrary to the observed speckled distribution of some other transcription factors, e.g., STAT1 (31), or

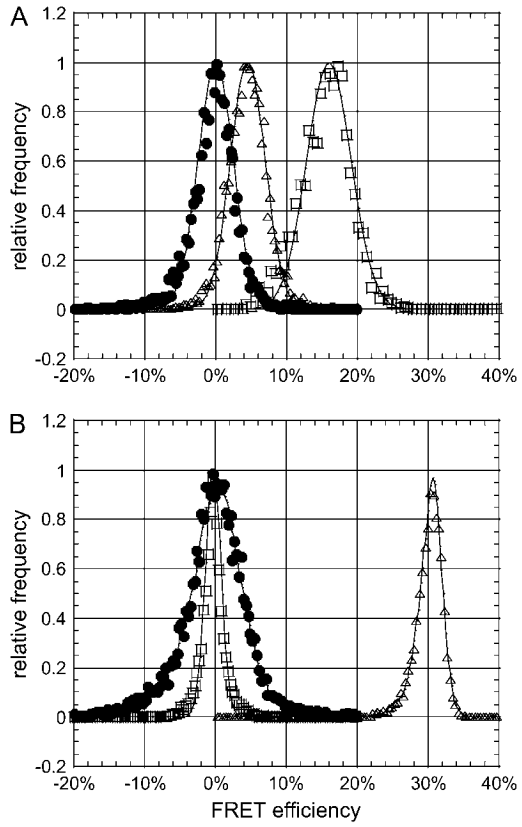

FIGURE 3 Normalized frequency distribution histograms of mean cellular FRET efficiencies measured by flow cytometry as determined from >20,000 cells. (*A*) Nonassociating Fos-EGFP+JunΔ-mRFP1 (*circles*), full-length Fos-EGFP+Jun-mRFP1 (*triangles*), and truncated Fos^{215}-EGFP+Jun-mRFP1 (*squares*). (*B*) Negative controls: separately expressed EGFP and mRFP1 (*circles*) and EGFP expressed alone (*squares*); positive control: EGFP-mRFP1 fusion protein (*triangles*).

liganded steroid receptors such as AR (32). The separately expressed EGFP and mRFP1 (*middle row*), the EGFP-mRFP1 fusion protein (*bottom row*), as well as JunΔ (not shown), were homogenously distributed in the cytoplasm and the nucleus. The nucleoli appear as a dark spot in every case. Even though the distribution of the individual transcription factor molecules is homogenous, their interaction could be influenced by the local environment. This raises an interesting question whether the dimerization of Jun and Fos occurs preferentially at specific nuclear compartments/gene segments, or their association state is independent of the exact localization within the nucleus. We found that the distributions of FRET efficiency values are rather homogeneous in the nucleus for the Fos^{215}-Jun heterodimer, such as for the positive and negative controls. The homogeneity is also reflected in the narrow distributions of the FRET histograms calculated from the pixel values of each image. This suggests that the association state of Jun and Fos and the conformation of the dimer do not depend crucially on the local environment in the nucleus or on the presence of specifically located DNA sequences. The average FRET efficiencies for the Fos-Jun ($3.0 \pm 1\%$), Fos^{215}-Jun ($9.9 \pm 0.5\%$), Fos-JunΔ pairs ($-0.4 \pm 1.4\%$), the EGFP-mRFP1 fusion proteins ($22.1 \pm 2.8\%$), and the separately coexpressed EGFP and mRFP1 dyes ($0.3 \pm 0.8\%$) were determined from ~30–80 cells. The FRET efficiencies determined by confocal microscopy are systematically lower than those determined by FACS even for the controls (Table 1). This may partially be due to more pronounced photobleaching during imaging, which reduces the number of acceptors available for FRET. In addition, cell-by-cell and pixel-by-pixel calculations differently weight high- and low-intensity regions in the same cell, skewing pixel-FRET histograms toward lower FRET efficiencies (33).

FCCS

Earlier we have shown the stable association and DNA binding of full-length Fos and Jun by FCCS (18). We also performed FCCS measurements on cells transfected with the Fos^{215} and Jun to determine whether the truncation of the Fos protein at the C-terminal influences the dimerization, mobility, or DNA binding of the constructs. The extent of dimerization is monitored by the cross-correlation amplitude; the mobility of the different species is inferred from the diffusion times, whereas the percentage of DNA bound dimer can be assessed from the fraction of the slow component. Fig. 5 shows normalized autocorrelation curves and the cross-correlation between the two species. The presence of cross correlation proves that there is stable interaction between these constructs. The cross-correlation amplitude calculated as a percentage of the autocorrelation amplitude of the green channel was $34 \pm 6\%$. This value is close to that found earlier for the full-length Fos and Jun ($31 \pm 6\%$), and is significantly different from the negative control (separately expressed EGFP and mRFP1: $13 \pm 3\%$, arising from the spectral crosstalk of the EGFP signal into the red detection channel (18)). Although the influence of FRET complicates the direct comparison of the relative cross-correlation amplitudes (34), these data clearly indicate that the dimerization is not considerably affected by the truncation. There are two components present in the auto- and cross-correlation signals; the fast one has diffusion times ranging from 1.0 to 1.4 ms, whereas the slow one, 67–91 ms on average, is similar to those published earlier for the full-length constructs. The two components can be attributed to the free and DNA-bound proteins. The long diffusion times may also mean average residence times of the Jun-Fos complex spent in a DNA-bound state. The fraction of the slow component in the cross-correlation curves is $56 \pm 4\%$ for the Fos^{215}-Jun complex, whereas it was $\sim 77 \pm 13\%$ in the case of the full-length Fos-Jun construct. The decrease in the fraction of the slower component may suggest that the C-terminal domain, which was deleted from the full-length Fos-EGFP, might be involved in anchoring the dimer to other nuclear components. This is concordant with a possible transactivation role of this C-terminal domain observed in the transformation of fibroblasts (35).

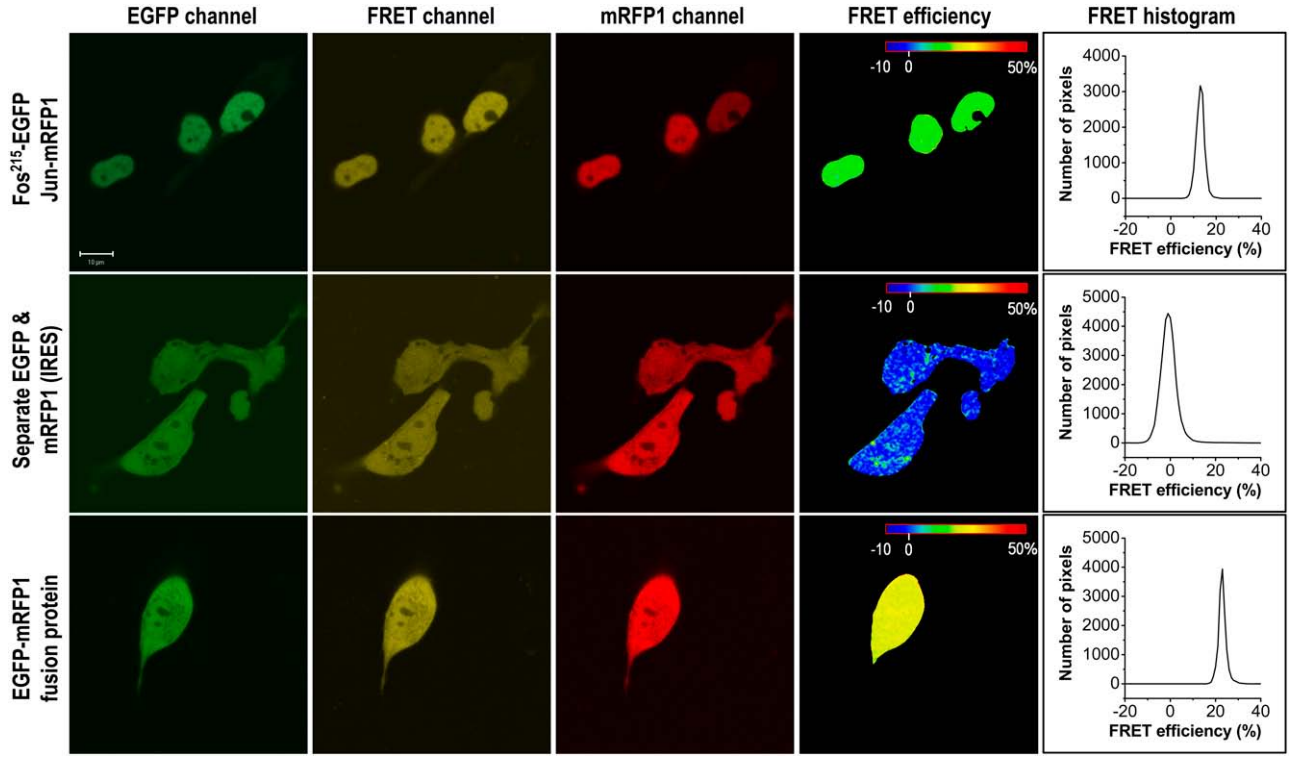

FIGURE 4 FRET experiments on HeLa cells using confocal microscopy. Confocal sections were recorded from 1.5-μm-thick optical slices of the cells. (*Top row*) Cells expressing Fos^{215}-EGFP and Jun-mRFP1 (note nuclear localization); (*middle row*) separately expressed EGFP and mRFP1 (negative control); (*bottom row*) EGFP-mRFP1 fusion protein (positive control). The EGFP channel (*green*) contains pure donor signal quenched by FRET (excitation: 488 nm; emission: 505–550 nm). The signal in the FRET channel (*yellow*) has contributions from the sensitized as well as directly excited emission of mRFP1 and crosstalk from EGFP (excitation: 488 nm; emission: 560–610 nm). The mRFP1 channel (*red*) contains the directly excited emission of the acceptor (excitation: 543 nm; emission: 560–610 nm). From these signals, the FRET efficiency between the EGFP and mRFP1 labels was calculated in each pixel as described, and its subcellular distribution is displayed in the FRET efficiency images. From these images frequency distribution histograms were also created, displaying mean FRET efficiencies of 13.0% (Fos^{215}-Jun), −0.7% (negative control), and 23.0% (positive control) for these particular cells. All colors used in the figure are pseudocolors. Scale bar: 10 μm.

It is noteworthy that FCCS and FRET measurements probe two different extremes of the total cell population with respect to expression levels. For the FCCS experiments, cells with lower expression levels were used; for FRET, cells with high expression were selected to produce reliable FRET values. Thus, the two methods are complementary in the sense of being applicable in different concentration regimes. Consequently, the extent of association between Fos and Jun as measured by the two methods is expected to be different: in the population analyzed by FRET, especially at higher N_A/N_D values, the reaction is probably shifted toward association as compared to the population analyzed by FCCS. While FCCS elucidates dynamic and stability parameters of the association reaction, FRET yields information on the equilibrium parameters of the formed complex(es).

Molecular dynamics (MD) modeling of the Fos-Jun complexes

To relate the FRET-measured distances to possible molecular structures of the dimer, MD modeling was carried out. The first complex analyzed was the truncated Fos^{215}-EGFP + Jun-mRFP1 dimer downstream of the DNA binding domains.

TABLE 1 FRET efficiencies (*E*) and estimated donor-acceptor distances (*d*)

	Flow cytometry		Confocal microscopy		
	E (%)	*d* (nm)	*E* (%)	*d* (nm)	Modeling
Fos-Jun	4 ± 0.5%	(8 ± 1 nm)	3.0 ± 1%	(8.4 ± 0.5 nm)	6–20 nm
Fos^{215}-Jun	17 ± 1%	(6.1 ± 1 nm)	9.9 ± 0.5%	(6.8 ± 0.1 nm)	6.7 ± 0.1 nm
Fos-JunΔ	0.5 ± 1%		−0.4 ± 1.4%		
EGFP-mRFP1 fusion	30 ± 1%	(5.4 ± 0.5 nm)	22.1 ± 2.8%	(5.8 ± 0.15 nm)	
EGFP and mRFP1	0.2 ± 2%		0.3 ± 0.8%		

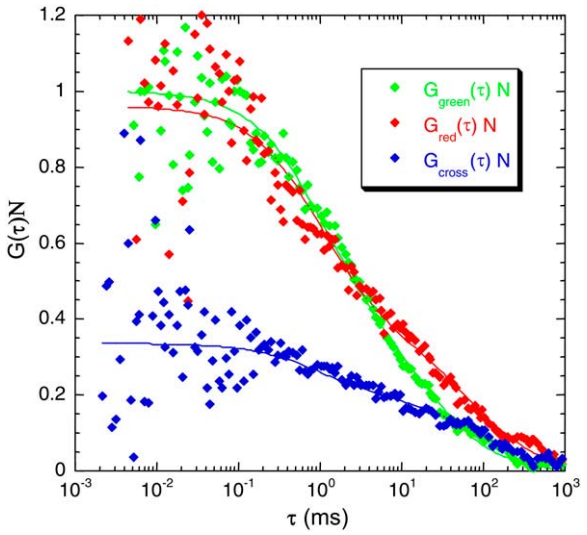

FIGURE 5 Normalized autocorrelation and cross-correlation curves of Fos^{215}-EGFP and Jun-mRFP1. The curves were fit to a model assuming two distinct diffusing components: a fast species corresponding to unbound (monomeric or dimeric) proteins, and a slow one corresponding presumably to proteins bound to nuclear elements.

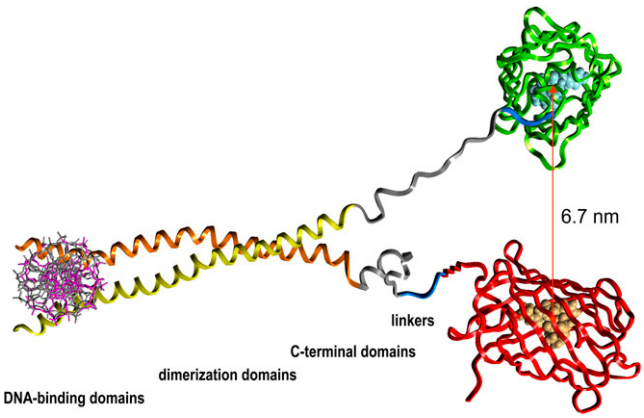

FIGURE 6 Relaxed MD model of the Fos^{215}-EGFP + Jun-mRFP1 complex downstream of the DNA binding domains. Chromophores are marked by bright green and red. The distance between the Glu-A339 (*red*) and Thr-C288 (*green*) is 6.7 nm.

The resulting three-dimensional model of the relaxed complex is presented in Fig. 6. The domains are denoted by the same color code as that used in Fig. 1. The chromophores (marked by *bright colors* in the figure) are ~6.7 nm apart, in excellent agreement with the FRET result (6.1 ± 1 nm). Starting from this conformation, we simulated the time dependence of the Fos^{215}-EGFP + Jun-mRFP1 complex over a 550-ps period. Despite the bulky fluorescent proteins, the AP-1 dimer remained stable, and only some local rearrangements were observed leading to short deviations from its ideal helical structure. To estimate the space between the mRFP1 and the EGFP chromophores, the distances between the Cα atoms of Pro-398 (mRFP1) and Thr-288 (EGFP), which are located in the center of each chromophore, were calculated. As can be seen in Fig. 7, the distance between the two chromophores is rather invariable (SD = 0.13 nm). Theoretically, the maximal distances between the centers of the two chromophores corresponding to a fully stretched peptide chain can be estimated to be in the range of 14–15 nm; whereas the closest possible distance, in which the outer spheres of the two β-barrels of the fluorescent proteins form van der Waals contacts, would be 3–3.5 nm. The distance of the chromophores relative to the complete Fos^{215}-Jun complex showed larger deviations than that between the chromophores (7.4 ± 0.32 nm between Glu-310 (Jun) and Pro-398 (mRFP1), and 8.7 ± 0.35 nm between Leu-197 (Fos) and Thr-288 (EGFP)).

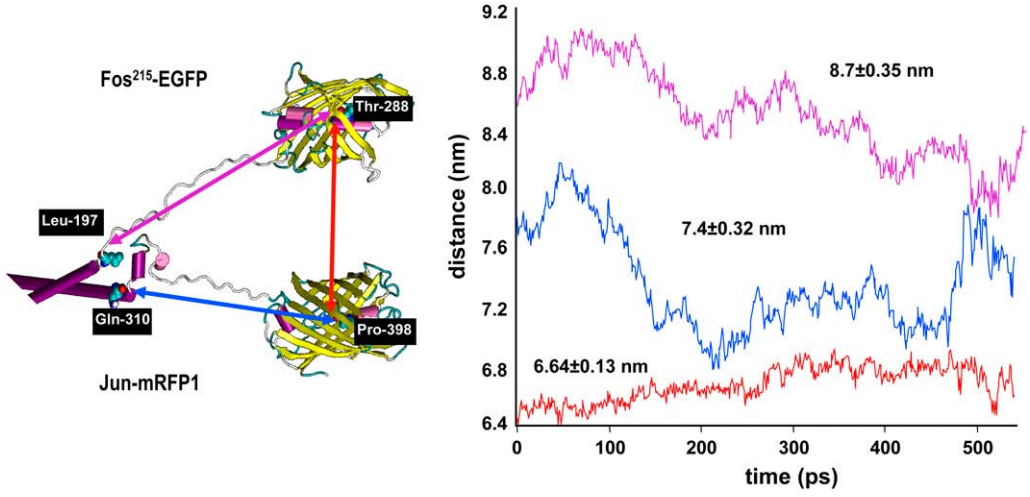

FIGURE 7 Simulated distance fluctuations between selected residues of the Fos^{215}-EGFP:Jun-mRFP1 complex over a period of 500 ps. Importantly, the dimer remained stable. The distance between the EGFP and mRFP1 (*red arrow* and *curve*) shows little deviation (SD = 0.13 nm). The separation between EGFP and Fos (*purple*), as well as mRFP1 and Jun (*blue*), shows somewhat larger variations (SD = 0.35 nm and 0.32 nm, respectively).

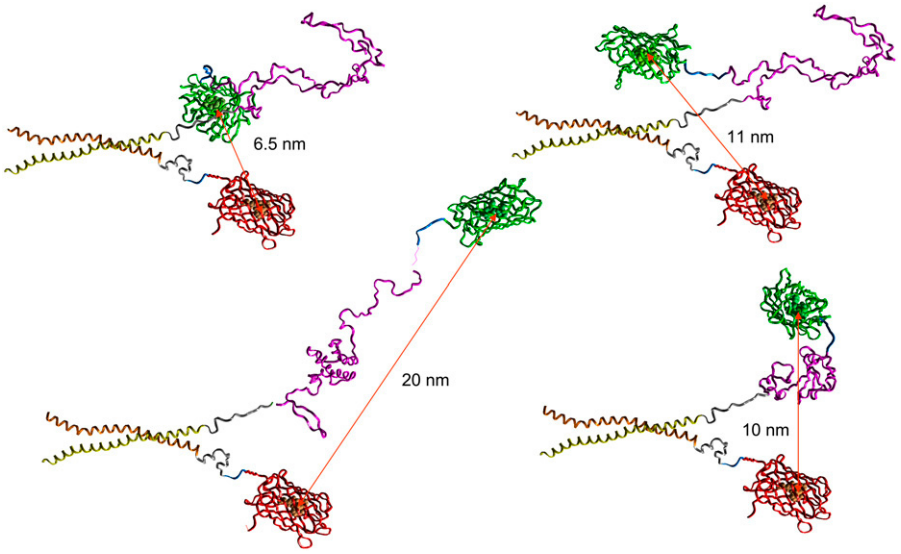

FIGURE 8 Four possible conformations of the full-length Fos-Jun dimer downstream of the DNA-binding domains. Predictions showed little or no similarity, with dye-to-dye distances varying between 6.5 and 20 nm. The mean FRET efficiency (4 ± 0.5%) corresponds to an average distance of 8 ± 1 nm. Thus, more compact conformations are probably dominant in the population.

We also modeled the full-length Fos-EGFP + Jun-mRFP1 complex downstream of the DNA binding domains. The results of all secondary structure prediction services were consistent in not being able to predict any three-dimensional fold or pronounced secondary structure regions for the C-terminal of the full-length Fos. Most of the sequence homology-based modeling services failed to predict three-dimensional protein structures. The sequence similarity to all known three-dimensional proteins structures is so low that no reliable model can be generated. Only Agape, a profile-profile alignment method (36), and the Wurst service (37) using a threading approach with a structural scoring function and sequence profiles, sent back five suggestions each. A visual inspection of the 10 received models displayed no common structural motifs and they covered a wide range of potential solutions. To demonstrate the minimal and maximal elongation of the C-terminal domain of Fos, four models are presented: those exhibiting the longest and closest stretch between the N- and C-terminal residues, and two structures with a medium long stretch (Fig. 8). These conformations were optimized as described in Materials and Methods. Dye-to-dye distances in these models vary between 6 and 20 nm. We can compare the theoretically possible distances with our FRET-determined average value (8 nm). The applied methods do not resolve the distribution of FRET efficiencies in the population. However, considering the strong distance dependence of FRET, we can conclude that the majority of the complexes are in states characterized by shorter dye-to-dye distances (<10 nm).

This example shows that MD modeling predictions are reliable only if the sequence determines known secondary structural elements or if structural information for a homologous sequence is already available as in the case of Fos^{215}. Such information is not available for the C-terminal segment of the full-length Fos; thus, experimental data are required to justify MD-modeled structures.

A more detailed picture of the Fos-Jun complex

Our new robust FRET evaluation method allows for the precise assessment of dye-to-dye distances in the studied complexes. For Fos^{215}-EGFP + Jun-mRFP1 dimer our dye-to-dye distance estimation (6.1 ± 1 nm) from flow cytometric cell-by-cell FRET measurement was in good agreement with the prediction of MD modeling (6.7 ± 0.1 nm). An earlier photobleaching FRET study (14) reported a FRET efficiency of 7.5% between the N-termini. Assuming a Förster radius of ~5 nm for the CFP-YFP donor-acceptor pair (38), this corresponds to a distance of ~7.6 nm. Thus, the N-terminal segments preceding the DNA binding domains are not parallel; instead, they assume a more compact conformation, related to the function of the transactivation domains, e.g., binding to a common interaction partner. Similar to this observation, our FRET results imply that the C-terminal ends of Jun and full-length Fos are also within the range of energy transfer. Thus, we are able to constrain the possible range of conformations allowed by MD modeling, at least for the majority of the population, to those in a less extended state (dye-to-dye distance between 6 and 10 nm). This may also suggest that the C-terminal domains bind to adjacent nuclear components. The C-terminal end of Fos may play a role in the stabilization of the interaction between AP-1 and DNA. A possible contribution of the C-terminal domains to binding to nuclear elements is corroborated by our FCCS results, since truncation of Fos reduced the fraction of the slow component in our FCCS studies. Clarification of this assumption requires further biochemical and functional studies.

This article is dedicated to the memory of Dr. Claus-Wilhelm von der Lieth, our highly respected and beloved colleague.

The c-Jun and c-Fos genes were donated by P. Angel and F. Rösl (DKFZ, Heidelberg). The plasmid for mRFP1 was a kind gift of R. Tsien (University of California at San Diego). The authors wish to thank Dr. Aaron Hieb for useful comments on the manuscript.

This research was funded by the Hungarian National Scientific Research Fund (grants No. NK61412, No. T48745), the Health Scientific Committee (grants No. 2006/070, No. 2006/065), and the German Academic Exchange Service and Hungarian Fellowship Committee (grant No. 2006/34). N.B. and G.V. were recipients of an EMBO short-term fellowship. G.V. was a recipient of a Bolyai Research Fellowship.

REFERENCES

1. Chinenov, Y., and T. K. Kerppola. 2001. Close encounters of many kinds: Fos-Jun interactions that mediate transcription regulatory specificity. *Oncogene*. 20:2438–2452.
2. Vogt, P. K. 2001. Jun, the oncoprotein. *Oncogene*. 20:2365–2377.
3. Malnou, C. E., T. Salem, F. Brockly, H. Wodrich, M. Piechaczyk, and I. Jariel-Encontre. 2007. Heterodimerization with JUN family members regulates c-Fos nucleocytoplasmic traffic. *J. Biol. Chem.* 282:31046–31059.
4. Glover, J. N., and S. C. Harrison. 1995. Crystal structure of the heterodimeric bZIP transcription factor c-Fos-c-Jun bound to DNA. *Nature*. 373:257–261.
5. Weidemann, T., M. Wachsmuth, T. A. Knoch, G. Muller, W. Waldeck, and J. Langowski. 2003. Counting nucleosomes in living cells with a combination of fluorescence correlation spectroscopy and confocal imaging. *J. Mol. Biol.* 334:229–240.
6. Bacia, K., S. A. Kim, and P. Schwille. 2006. Fluorescence cross-correlation spectroscopy in living cells. *Nat. Methods.* 3:83–89.
7. Vámosi, G., A. Bodnár, G. Vereb, A. Jenei, C. K. Goldman, J. Langowski, K. Tóth, L. Mátyus, J. Szöllösi, T. A. Waldmann, and S. Damjanovich. 2004. IL-2 and IL-15 receptor α-subunits are coexpressed in a supramolecular receptor cluster in lipid rafts of T cells. *Proc. Natl. Acad. Sci. USA.* 101:11082–11087.
8. Clegg, R. M. 1995. Fluorescence resonance energy transfer. *Curr. Opin. Biotechnol.* 6:103–110.
9. Damjanovich, S., R. Gáspár, Jr., and C. Pieri. 1997. Dynamic receptor superstructures at the plasma membrane. *Q. Rev. Biophys.* 30:67–106.
10. Hink, M. A., T. Bisselin, and A. J. Visser. 2002. Imaging protein-protein interactions in living cells. *Plant Mol. Biol.* 50:871–883.
11. Jares-Erijman, E. A., and T. M. Jovin. 2003. FRET imaging. *Nat. Biotechnol.* 21:1387–1395.
12. Nagy, P., L. Bene, W. C. Hyun, G. Vereb, M. Braun, C. Antz, J. Paysan, S. Damjanovich, J. W. Park, and J. Szöllösi. 2005. Novel calibration method for flow cytometric fluorescence resonance energy transfer measurements between visible fluorescent proteins. *Cytometry A*. 67:86–96.
13. Trón, L., J. Szöllösi, S. Damjanovich, S. H. Helliwell, D. J. Arndt-Jovin, and T. M. Jovin. 1984. Flow cytometric measurement of fluorescence resonance energy transfer on cell surfaces. Quantitative evaluation of the transfer efficiency on a cell-by-cell basis. *Biophys. J.* 45:939–946.
14. Camuzeaux, B., C. Spriet, L. Heliot, J. Coll, and M. Duterque-Coquillaud. 2005. Imaging Erg and Jun transcription factor interaction in living cells using fluorescence resonance energy transfer analyses. *Biochem. Biophys. Res. Commun.* 332:1107–1114.
15. Hu, C. D., Y. Chinenov, and T. K. Kerppola. 2002. Visualization of interactions among bZIP and Rel family proteins in living cells using bimolecular fluorescence complementation. *Mol. Cell.* 9:789–798.
16. Kerppola, T. K. 2006. Visualization of molecular interactions by fluorescence complementation. *Nat. Rev. Mol. Cell Biol.* 7:449–456.
17. Kerppola, T. K. 2006. Complementary methods for studies of protein interactions in living cells. *Nat. Methods.* 3:969–971.
18. Baudendistel, N., G. Müller, W. Waldeck, P. Angel, and J. Langowski. 2005. Two-hybrid fluorescence cross-correlation spectroscopy detects protein-protein interactions in vivo. *ChemPhysChem.* 6:984–990.
19. Knippers, R. 1997. Molecular Genetics. Thieme Verlag, Stuttgart, Germany.
20. Patterson, G. H., S. M. Knobel, W. D. Sharif, S. R. Kain, and D. W. Piston. 1997. Use of the green fluorescent protein and its mutants in quantitative fluorescence microscopy. *Biophys. J.* 73:2782–2790.
21. Szentesi, G., G. Horváth, I. Bori, G. Vámosi, J. Szöllösi, R. Gáspár, S. Damjanovich, A. Jenei, and L. Mátyus. 2004. Computer program for determining fluorescence resonance energy transfer efficiency from flow cytometric data on a cell-by-cell basis. *Comput. Methods Programs Biomed.* 75:201–211.
22. Tewes, M. 1998. Experimental setup for fluorescence correlation spectroscopy, extension of the theoretical bases and biological applications. PhD thesis. Ruprecht-Karls-Universität, Heidelberg, Germany.
23. Wachsmuth, M. 2001. Fluorescence fluctuation microscopy: prototype development, theory and measurement of intranuclear mobility of biomolecules. PhD thesis. Ruprecht-Karls-Universität, Heidelberg, Germany.
24. Wachsmuth, M., W. Waldeck, and J. Langowski. 2000. Anomalous diffusion of fluorescent probes inside living cell nuclei investigated by spatially resolved fluorescence correlation spectroscopy. *J. Mol. Biol.* 298:677–689.
25. Yarbrough, D., R. M. Wachter, K. Kallio, M. V. Matz, and S. J. Remington. 2001. Refined crystal structure of DsRed, a red fluorescent protein from coral, at 2.0-Å resolution. *Proc. Natl. Acad. Sci. USA.* 98:462–467.
26. Yang, F., L. G. Moss, and G. N. Phillips, Jr. 1996. The molecular structure of green fluorescent protein. *Nat. Biotechnol.* 14:1246–1251.
27. Arnold, K., L. Bordoli, J. Kopp, and T. Schwede. 2006. The SWISS-MODEL workspace: a web-based environment for protein structure homology modeling. *Bioinformatics.* 22:195–201.
28. Van Der Spoel, D., E. Lindahl, B. Hess, G. Groenhof, A. E. Mark, and H. J. Berendsen. 2005. GROMACS: fast, flexible, and free. *J. Comput. Chem.* 26:1701–1718.
29. Peter, M., S. M. Ameer-Beg, M. K. Hughes, M. D. Keppler, S. Prag, M. Marsh, B. Vojnovic, and T. Ng. 2005. Multiphoton-FLIM quantification of the EGFP-mRFP1 FRET pair for localization of membrane receptor-kinase interactions. *Biophys. J.* 88:1224–1237.
30. Campbell, R. E., O. Tour, A. E. Palmer, P. A. Steinbach, G. S. Baird, D. A. Zacharias, and R. Y. Tsien. 2002. A monomeric red fluorescent protein. *Proc. Natl. Acad. Sci. USA.* 99:7877–7882.
31. Tan, J. A., S. H. Hall, K. G. Hamil, G. Grossman, P. Petrusz, and F. S. French. 2002. Protein inhibitors of activated STAT resemble scaffold attachment factors and function as interacting nuclear receptor coregulators. *J. Biol. Chem.* 277:16993–17001.
32. Saitoh, M., R. Takayanagi, K. Goto, A. Fukamizu, A. Tomura, T. Yanase, and H. Nawata. 2002. The presence of both the amino- and carboxyl-terminal domains in the AR is essential for the completion of a transcriptionally active form with co activators and intranuclear compartmentalization common to the steroid hormone receptors: a three-dimensional imaging study. *Mol. Endocrinol.* 16:694–706.
33. Nagy, P., G. Vámosi, A. Bodnár, S. J. Lockett, and J. Szöllösi. 1998. Intensity-based energy transfer measurements in digital imaging microscopy. *Eur. Biophys. J.* 27:377–389.
34. Hom, E. F., and A. S. Verkman. 2002. Analysis of coupled bimolecular reaction kinetics and diffusion by two-color fluorescence correlation spectroscopy: enhanced resolution of kinetics by resonance energy transfer. *Biophys. J.* 83:533–546.
35. Wisdom, R., and I. M. Verma. 1993. Transformation by Fos proteins requires a C-terminal transactivation domain. *Mol. Cell. Biol.* 13:7429–7438.
36. Przybylski, D., and B. Rost. 2004. Improving fold recognition without folds. *J. Mol. Biol.* 341:255–269.
37. Torda, A. E., J. B. Procter, and T. Huber. 2004. Wurst: a protein threading server with a structural scoring function, sequence profiles and optimized substitution matrices. *Nucleic Acids Res.* 32:W532–W535.
38. Tsien, R. Y. 1998. The green fluorescent protein. *Annu. Rev. Biochem.* 67:509–544.